J. Fluid Mech. (1976), *vol.* 77, *part* 4, *pp.* 769–788
Printed in Great Britain

Baroclinic instability in an eccentric annulus

By P. R. GENT

Department of Oceanography, University of Southampton, England†

AND H. LEACH

Geophysical Fluid Dynamics Laboratory, Meteorological Office, Bracknell, Berkshire, England‡

(Received 23 December 1974 and in revised form 11 June 1976)

A study has been made of baroclinic instability in a differentially heated, rotating fluid annulus whose channel width varies azimuthally. Both laboratory experiments and an analytical model employing a linear normal-mode analysis have been used. The experiments show three types of flow. For slow rotation the flow is 'symmetric', whereas at high rotation speeds baroclinic waves occur at all azimuths. At intermediate rotation speeds it is possible to have a mixed flow which is 'symmetric' in the narrow part but has baroclinic waves in the wide part of the annulus. This result suggested the analytical investigation of the stability of a baroclinic flow whose meridional scale varies downstream. It was found that this model also permits three possible types of flow: everywhere stable, everywhere unstable, and also a mixed flow which is locally unstable where the meridional scale is largest but locally stable where the scale is smallest.

1. Introduction

In this paper we extend the baroclinic-instability work of the last 25 years to the case of an eccentric annulus. Early experiments (Fultz 1949, 1951; Hide 1953, 1958) showed that, when an annulus of water was rotated about its vertical axis of symmetry and a radial temperature difference applied, various flow regimes occurred according to the values of the rotation speed and temperature difference. In particular, at low rotation speeds (for a given temperature difference) the flow in the interior region of the fluid was axisymmetric, but above a critical speed a pattern of baroclinic waves was set up. Beyond another critical speed the flow pattern was found to be irregular. Subsequently more investigations were carried out (for example, Fultz *et al.* 1959; Fowlis & Hide 1965) to determine the extent of the different flow regimes in parameter space. These and other investigations have been reviewed by Hide & Mason (1975).

The first analytical models of baroclinic instability (Charney 1947; Eady 1949) were made with the atmosphere in mind. An inviscid fluid in a straight channel rotating about the vertical and bounded above and below by rigid surfaces formed

† Present address: N.C.A.R. Boulder, Colorado 80303.
‡ Present address: Department of Oceanography, University of Southampton.

the basis of Eady's model. Using what would now be termed the quasi-geostrophic approximation, he obtained a simple equation for the perturbation quantities of a linear stability analysis. The equation derived (see Phillips 1963; Hide 1969) contains a dimensionless parameter B whose square root is the Rossby radius of deformation divided by the width of the annulus and which measures the importance of stratification as against Coriolis effects. When normal modes were taken, the resulting eigenvalue problem showed that in Eady's model all the modes were stable if $B > 0{\cdot}583$ but if B was below this critical value long waves were unstable and short waves stable. Comparisons of these results with annulus experiments show reasonable agreement for low viscosity considering the neglect of details of curvature, flow structure and nonlinear effects. Later workers (Davies 1956; Brindley 1960; Williams 1974; Pedlosky 1970; Drazin 1970) confirmed that such approximations did not substantially alter Eady's result, provided that potential-vorticity gradients are absent from the interior of the fluid. If such gradients are present in the basic flow it is possible for the short waves to be destabilized (Bretherton 1966; McIntyre 1970), but the effect appears to be weak enough to be nullified by comparatively small viscous dissipation (Barcilon 1964). In summary, it appears that Eady's simple model does provide the essential explanation, as originally proposed by Lorenz (1953) and Davies (1953), of the transition between axisymmetric and non-axisymmetric flow as the onset of baroclinic instability.

In the laboratory experiments described below, traverses were made across parameter space to find the positions at which waves could first be detected at both the widest and the narrowest point of the annulus. These experiments show that, within the range of conditions investigated, the instability is predominantly a local effect. This means that the nature of the flow at any point in the annulus is determined by the local values of the dimensionless parameters. Thus, in addition to the well-known 'symmetric' and wave regimes a new, intermediate mixed regime was found where both flow types could exist simultaneously in different parts of the annulus: waves in the wider section and 'symmetric' flow in the narrower section. Since only two traverses were made, using a water–glycerol solution and a silicone fluid, it was not possible to determine whether the transition curves on the regime diagram tend to a single inviscid limit, which would imply that, in this limit, the instability is entirely a local effect.

The mathematical model modifies Eady's inviscid theory to take account of the eccentricity of the annulus. Instead of assuming a spatially periodic solution along the channel, a JWKB solution is used which permits spatial oscillations in the wider part of the flow with exponentially damped solutions elsewhere. Although precise quantitative comparisons of the results of the two parallel investigations are inappropriate, both show the mixed flow regime occurring between the fully 'symmetric' and wave regimes. For this reason we felt justified in presenting the results of both investigations together. The paper proceeds with a discussion of the experiments and their results, after which follows the mathematical model and its results.

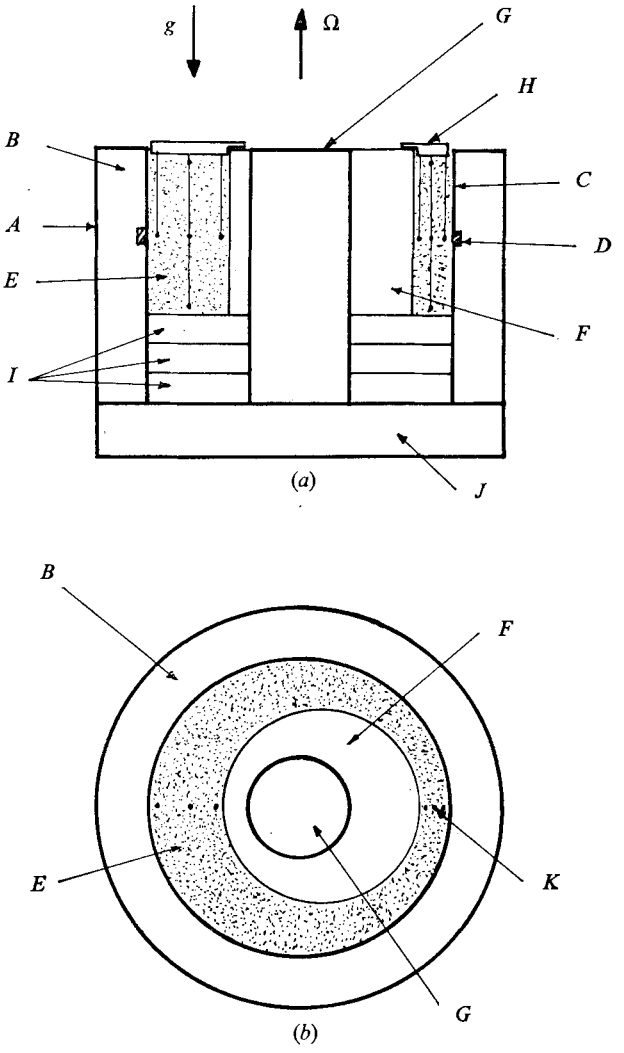

FIGURE 1. Diagram of experimental apparatus. (*a*) Side view. (*b*) Plan view. *A*, acrylic cylinder; *B*, outer temperature bath; *C*, copper outer wall; *D*, acrylic window; *E*, working fluid; *F*, eccentric light-alloy sleeve; *G*, brass cylinder containing inner temperature bath; *H*, acrylic lid with suspended thermocouple probes; *I*, acrylic false bases; *J*, phenolic laminate base; *K*, position of thermocouple probes.

2. Laboratory experiments: apparatus and procedure

The apparatus (see figure 1) was similar to that used in previous annulus experiments (for example Douglas, Hide & Mason 1972). Metal cylinders forming an annular region contained the working fluid. An eccentric sleeve made from light alloy fitted tightly onto the concentric brass inner cylinder to form the inner wall.

The depth of the working region was set at 122 mm using a system of false bases and the eccentric sleeve (see figure 1). This positioned the narrow window

near the mid-level of the fluid for streak photography (see Douglas *et al.* 1972) at a level of small azimuthal flow velocities. The working fluid used was either a 15 % solution of glycerol in water of viscosity 1·32 $mm^2 s^{-1}$ containing neutrally buoyant polystyrene beads or a silicone fluid of viscosity 0·65 $mm^2 s^{-1}$ containing a suspension of aluminium powder. The Prandtl numbers of these two fluids are 10·2 and 6·77 respectively so changing the fluid did not make a large change in this parameter. The thermal expansion coefficient of the silicone fluid is about five times larger than that of the water–glycerol solution but since the parameter B_L (see § 3) was calculated using density this difference was accounted for.

Two arrays of five thermocouples were used to measure the temperature within the fluid, one array at the widest and the other at the narrowest point of the channel (see figure 1). At the points where the temperature was to be measured 125 μm copper wires were soldered to 250 μm constantan vertical wires which were relatively rigid and suspended from the acrylic lid. The reference temperature in this experiment was the cold bath's temperature, the common return copper wire and the constantan wires from each of the thermocouples being soldered together to form a junction against the inside of the cold bath's wall. From the annulus the copper wires were joined to a screened cable which carried the signals to the top of the tripod, where a high-quality electrical slip-ring transferred them off the rotating system. Further screened cable carried the signals to a data logging system which could scan the channels at a preselected interval, and record the voltages measured in digital form. An analog signal was also available for continuous monitoring of a single channel on a chart recorder. This was used to see whether the working fluid had reached a steady state. From the trace produced it could be seen whether the temperature was steady, as with symmetric flow, or periodically varying, as with waves. In the latter case the sampling frequency was decided from the trace so that no information would be lost by aliasing of high frequencies to lower ones. The data were recorded on punched tape and logging continued for sufficient time to allow several hundred samples to be taken, to provide a good quantity of data for averaging. If drifting waves were present several wave lobes were allowed to move past the stationary thermocouple arrays. Photographs were taken to correlate with the temperature measurements.

3. Experimental results

The local B and Taylor number are defined by

$$B_L = -\frac{gd^2(\partial\rho_0/\partial z)}{4\Omega^2\bar{\rho}L^2}, \quad Ta_L = \frac{4\Omega^2 L^5}{\nu^2 d},$$

where g is the acceleration due to gravity, d the annulus depth, $\bar{\rho}$ and $\partial\rho_0/\partial z$ the mean density and the locally measured density gradient, Ω the apparatus rotation speed, ν the viscosity and $L = q(b-a)$ the local gap width (see § 4 and figure 4). The results of the two series of experiments using the two different fluids are presented in table 1. For each run this shows B_L and Ta_L at the widest and narrowest points of the annulus and indicates whether the flow was symmetric or con-

		Narrow region			Wide region			
Run	Ω (rad s^{-1})	B_L	$Ta_L \times 10^{-6}$	Stable/ waves	B_L	$Ta_L \times 10^{-6}$	Stable/ waves	m
			Water–glycerol solution					
W1	0·962	1·377	0·141	*S*	0·434	2·31	*S*	0
W2	1·015	1·263	0·157	*S*	0·408	2·58	*S*	0
W3	1·054	1·148	0·169	*S*	0·363	2·78	*W*	1
W4	1·104	1·053	0·186	*S*	0·376	3·05	*W*	1
W5	1·175	0·943	0·210	*S*	0·308	3·45	*W*	1
W6	1·301	0·770	0·258	*S*	0·249	4·23	*W*	2
W7	1·431	0·640	0·312	*S*	0·210	5·12	*W*	2
W8	1·548	0·557	0·365	*S*	0·186	5·99	*W*	2
W9	1·636	0·499	0·408	*S*	0·163	6·70	*W*	2
W10	1·698	0·541	0·439	*W*	0·162	7·21	*W*	4
W11	1·827	0·408	0·508	*W*	0·140	8·34	*W*	4
W12	1·928	0·365	0·566	*W*	0·125	9·29	*W*	4
			Silicone fluid					
S1	1·640	2·327	1·68	*S*	0·768	27·5	*S*	0
S2	1·848	1·900	2·13	*S*	0·634	34·9	*S*	0
S3	2·040	1·567	2·59	*S*	0·521	42·6	*W*	1
S4	2·252	1·332	3·16	*S*	0·448	51·9	*W*	1
S5	2·493	1·036	3·87	*S*	0·356	63·6	*W*	2
S6	2·978	0·735	5·53	*S*	0·251	90·7	*W*	2
S7	3·396	0·565	7·19	*W*	0·194	118·0	*W*	3
S8	3·984	0·404	9·89	*W*	0·137	162·3	*W*	–

TABLE 1. Summary of experimental results near transitions

tained baroclinic waves. This and the number of waves m were determined by photographic observations made with each logged run and by use of the recorded data. In figure 2, these results are shown on a regime diagram where the points are plotted using the local gap width L, which affects both B_L and Ta_L, and the locally measured $\partial\rho_0/\partial z$, which affects only B_L. The error in the measured values of B_L and Ta_L was about 10 %, arising from the errors in measuring experimental quantities. This error is demonstrated by the values of B_L in table 1, which do not decrease monotonically for the water–glycerol solution in the narrow region.

Figure 2 shows that in the wide region the transition to wave flow occurred at about the same position in parameter space as was found in the concentric case; curve HM on figure 2 is taken from Hide & Mason (1970, figure 15). Our results indicate that the critical value of B_L depends upon Ta_L and, as in the concentric case, may not tend to an inviscid limit but may keep on increasing slowly; see Ketchum (1972) and Douglas & Mason (1973). Williams (1974) indicates that this behaviour can be modelled by an inviscid theory in which B and $\partial\bar{u}/\partial z$ are functions of z. Two pieces of evidence suggest that the instability observed initially in the wide region is not forced in any way. First, no waves occur whilst B_L at the widest point (i.e. the lowest B_L anywhere) exceeds that for the concentric-annulus transition. Second, the ability of the wave pattern to drift relative to

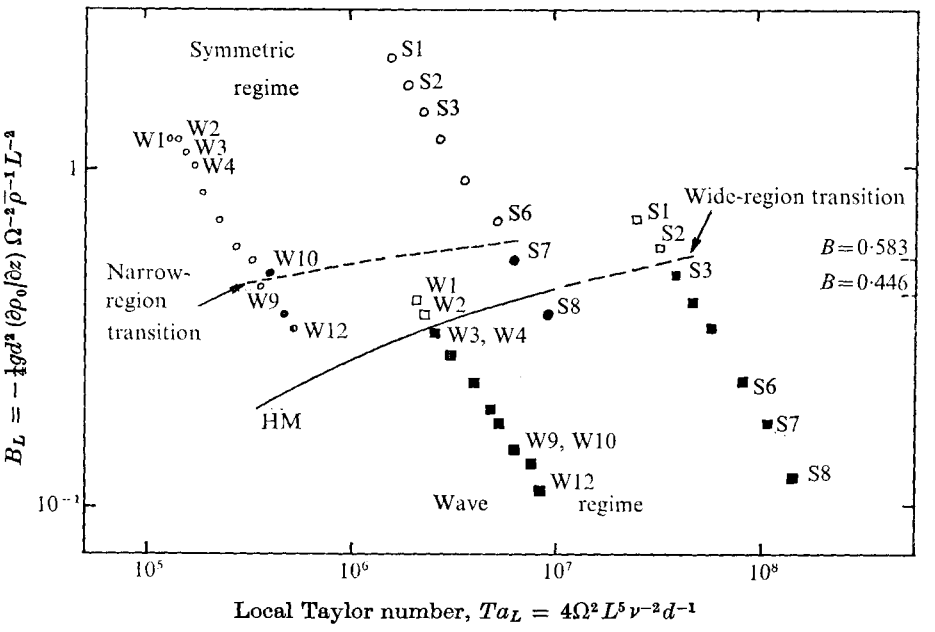

FIGURE 2. Experimental results plotted on a regime diagram. Narrow-region points: ○, stable; ●, waves. Wide region points: □, stable; ■, waves. HM, transition curve from Hide & Mason (1970). The run numbers indicate the values in table 1.

the boundaries implies that its exact form is not being controlled closely by the boundary conditions (as is the case, for example, with localized bottom topography; Leach 1975). The waves seen first in the wide region are a result of local instability which spreads to the rest of the annulus as the local values of B_L decrease.

If the onset of instability in the narrow region of the annulus were purely local then the transition curves on figure 2 would be superimposed. If, however, instability occurred everywhere simultaneously (i.e. at the same value of Ω), the narrow-region transition curve would occur for values of B_L greater than 1·0 (see table 1) and thus the narrow-region transition curve would appear well above its actual position on the regime diagram, figure 2. In reality neither of these extremes is the case, but the curve is at distinctly higher values of B_L compared with the wide-region curve, showing a slight destabilization. So some non-local effect must be invoked to explain the more rapid spread (with decreasing B_L) of waves into the narrow region than would be expected if the instability were purely local. This could be advection of the waves from the unstable region into the narrow part of the annulus, or alternatively the proximity of the unstable region forcing waves where they would otherwise be viscously damped. The latter view is supported by the dependence of the effect on viscosity because the transition curves are closer together at high Ta_L. (We do not expect the curves to cross as $Ta_L \to \infty$ since this would imply stabilization of the narrow region for some non-viscous reason.) When waves do not occur in the narrow region, figure 2 shows that the values of Ta_L are well above the viscous cut-off for waves to occur. The

knee of the concentric-annulus curve occurs at $Ta \simeq 10^5$ (Fowlis & Hide 1965). Thus the absence of waves is due to the high values of B_L, and is not caused by viscous dissipation of the waves since Ta_L is well above 10^5.

The drift of the wave pattern relative to the annulus could be observed by both chart-recorder and computer-program representations of the temperature variation at a point and also by both still and ciné photography. From these it seemed that such drift was often inhibited in the eccentric annulus (compared with the concentric annulus) although some films and traces did show steady drifting of a wave pattern. Using the recorded data for those cases it was possible to study the vertical structure of the waves. In only one case was the temperature amplitude of the waves at the top and bottom of the channel sufficient to determine their relative phase but in that case it was 1·1 rad, in agreement with the experimental results of Douglas *et al.* (1972, figure 10). The data also show that the temperature amplitude of the waves is largest near the middle of the fluid, a feature of baroclinic waves in a concentric annulus (see Williams 1971). In addition to the transition occurring for B_L in the range 0·4–0·6, this phase and amplitude information indicates strongly that the observed waves were indeed baroclinic waves. Some photographs of the flow patterns observed at a variety of rotation speeds are presented in figure 3 (plates 1–5).

The waves could be made to drift by having a free upper surface to the working fluid. Such an asymmetry between the top and bottom boundary conditions causes the thermal-wind shear to give the fluid a net azimuthal velocity. Ciné films taken of drifting waves when only part of the eccentric annulus was unstable show that the waves grow where the channel widens, drift through the widest region and decay where the channel narrows, clearly indicating the region of baroclinic instability.

It would be desirable to conduct more experiments at even higher Taylor number although the value of 10^8 reached is higher than that of many workers (Fowlis & Hide 1965; Hide & Mason 1970). This would decide whether the two transition curves converge as Ta_L becomes large, consequently implying that the onset of instability is a purely local effect everywhere. However, such an investigation is not possible with the present apparatus; a larger annulus would need to be constructed.

4. Mathematical model

Equations of motion

At first sight it might seem desirable to use eccentric annular co-ordinates (see Wood 1957) in order to find the stability of the experimental flow described above. It was decided, however, to use Cartesians instead and to treat the flow as if it were in a channel of varying width, as the simplicity of the equations of motion outweighs the disadvantage of the asymmetric boundary condition at the inner cylinder. Cartesian co-ordinates (x', y', z') are related to cylindrical polar co-ordinates (r', θ, z') with origin at the centre of the outer cylinder by

$$y' = b - r', \quad x' = b\theta, \tag{1}$$

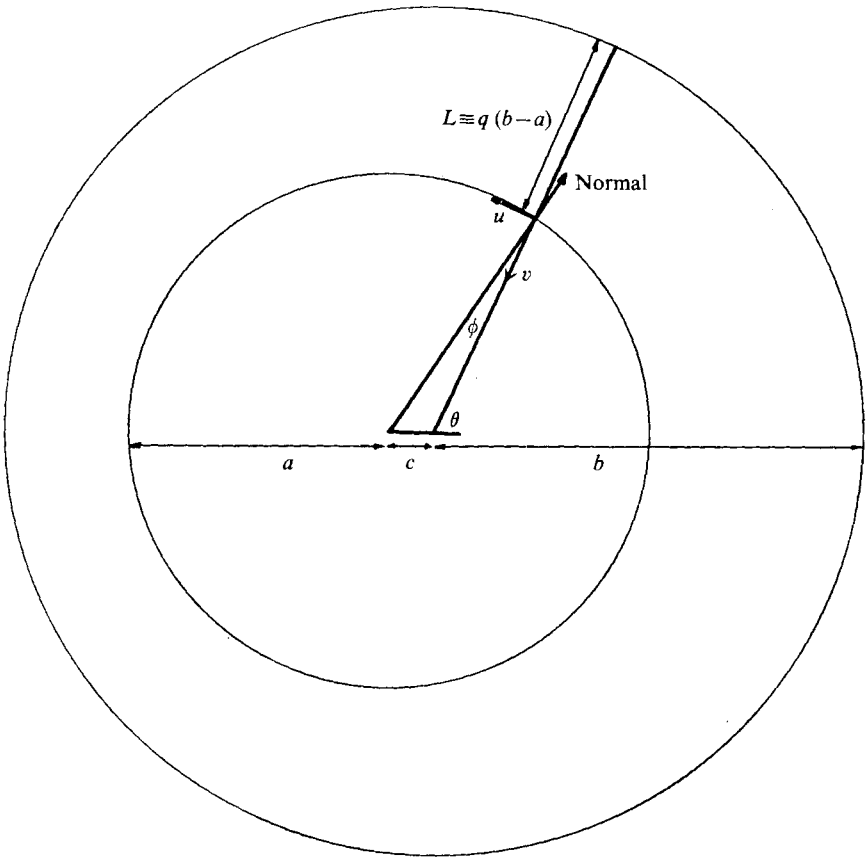

FIGURE 4. Plan view of eccentric annulus showing quantities used in mathematical analysis.

where a and b are the radii of the cylinders; see figure 4. If the annulus depth is d, non-dimensional co-ordinates can be defined by

$$(b-a)\,(x,y) = (x',y'), \quad dz = z'. \tag{2}$$

If we denote the distance between the cylinder centres by c and let the outer cylinder correspond to $y = 0$, then the inner cylinder, $y = q(\theta)$, is given by

$$q(\theta) = (b + c\cos\theta - a|\cos\phi|)/(b-a), \tag{3}$$

where
$$\sin\phi = (c/a)\sin\theta. \tag{4}$$

Let
$$\epsilon = (b-a)/b. \tag{5}$$

If ϵ is small curvature can be neglected and, since $\theta = \epsilon x$, q can be regarded as a slowly varying function of x.

The fluid is assumed to be incompressible, inviscid, adiabatic and Boussinesq and to be rotating about the vertical with angular velocity Ω. Non-dimensional velocities and time are defined by

$$V(u,v) = (u',v'), \quad VdRw/(b-a) = w', \quad (b-a)\,t/V = t', \tag{6}$$

where the Rossby number $R = V/2\Omega(b-a)$.

Following Pedlosky (1964), the equation for the pressure $\overline{p}$ of the basic flow is that for conservation of potential vorticity, namely

$$\frac{D_g}{Dt}\left[\frac{\partial^2\overline{p}}{\partial x^2}+\frac{\partial^2\overline{p}}{\partial y^2}+\frac{\partial}{\partial z}\left(\frac{1}{B}\frac{\partial\overline{p}}{\partial z}\right)\right]=0, \tag{7}$$

where $D_g/Dt = \partial/\partial t-(\partial\overline{p}/\partial y)\,\partial/\partial x+(\partial\overline{p}/\partial x)\,\partial/\partial y$, the geostrophic material derivative. Here B is taken to be a constant given by

$$B=-\frac{gd^2\partial\rho_0/\partial z}{4\Omega^2\overline{\rho}(b-a)^2}\equiv q^2B_L \tag{8}$$

(see Hide 1969), where B_L is the local value defined previously in §3. $\overline{p}$ can be expanded as a power series in ϵ, of which the first few terms are

$$\overline{p}=\frac{Bz^2}{2R}-yz\left(\frac{1}{q}-\epsilon\right)+\frac{\epsilon^2y^3z}{6}\frac{d^2}{d\theta^2}\left(\frac{1}{q}\right)+\epsilon^3yzf(\theta)+O(\epsilon^4). \tag{9}$$

The hydrostatic and geostrophic equations then give

$$\overline{T}=\frac{\partial\overline{p}}{\partial z}=\frac{Bz}{R}-y\left(\frac{1}{q}-\epsilon\right)+\frac{\epsilon^2y^3}{b}\frac{d^2}{d\theta^2}\left(\frac{1}{q}\right)+\epsilon^3yf+O(\epsilon^4), \tag{10}$$

$$\overline{u}=-\frac{\partial\overline{p}}{\partial y}=z\left(\frac{1}{q}-\epsilon\right)-\frac{\epsilon^2y^2z}{2}\frac{d^2}{d\theta^2}\left(\frac{1}{q}\right)-\epsilon^3zf+O(\epsilon^4), \tag{11}$$

$$\overline{v}=\frac{\partial\overline{p}}{\partial x}=\frac{\epsilon yz}{q^2}\frac{dq}{d\theta}+\frac{\epsilon^3y^3z}{b}\frac{d^3}{d\theta^3}\left(\frac{1}{q}\right)+\epsilon^4yz\frac{df}{d\theta}+O(\epsilon^5). \tag{12}$$

Thus $\overline{w}\equiv 0$ and, to lowest order in ϵ, $\overline{T}=R^{-1}Bz-q^{-1}y$, which agrees with the experimental situation, where the temperature difference across the annulus, at a given depth, is constant at all azimuths. A first-order differential equation can be found for the unspecified function $f(\theta)$ by imposing the boundary condition of zero normal velocity at the inner cylinder, namely

$$\overline{v}|\cos\phi|+\overline{u}\sin\phi=0 \quad \text{at} \quad y=q. \tag{13}$$

This basic flow has constant potential vorticity and so excludes the possibility of a slowly growing instability beyond the Eady cut-off. Such an instability can occur, as was shown by Charney (1947), Green (1960) and McIntyre (1970), when the potential-vorticity gradient is non-zero. This slowly growing instability of short waves is damped by viscosity in most annulus experiments, and the transition to waves found there should correspond qualitatively to the cut-off found in Eady's model.

Because the basic flow has constant potential vorticity, the perturbation pressure p satisfies (7) with D_g/Dt unaltered but with p replacing $\overline{p}$ in the expression for the potential vorticity. The boundary conditions of no normal flow at the

boundaries and matching of the pressure at the narrowest point are

$$v \equiv \partial p/\partial x = 0 \quad \text{on} \quad y = 0, \tag{14}$$

$$v|\cos\phi| + u\sin\phi \equiv \frac{\partial p}{\partial x}|\cos\phi| - \frac{\partial p}{\partial y}\sin\phi = 0 \quad \text{on} \quad y = q, \tag{15}$$

$$Bw \equiv -\left(\frac{\partial}{\partial t} + \bar{u}\frac{\partial}{\partial x} + \bar{v}\frac{\partial}{\partial y}\right)\frac{\partial p}{\partial z} + \left(\frac{\partial \bar{v}}{\partial z}\frac{\partial p}{\partial y} + \frac{\partial \bar{u}}{\partial z}\frac{\partial p}{\partial x}\right) = 0 \quad \text{on} \quad z = \pm\tfrac{1}{2}, \tag{16}$$

$$p(\theta = -\pi) = p(\theta = \pi). \tag{17}$$

When normal modes are taken and p is assumed proportional to $\exp(-i\omega t)$, equation (7) and the above boundary conditions define an eigenvalue problem for the complex constant ω. A separable solution can be found for p of the form

$$p = \left\{\sum_{r=0}^{\infty} \epsilon^r \psi_r(y, z, \theta)\right\} \chi(x, \epsilon)\, e^{-i\omega t}, \tag{18}$$

where

$$\omega = \sum_{r=0}^{\infty} \epsilon^r \omega_r. \tag{19}$$

Substituting in (7) and equating coefficients of powers of the small parameter ϵ, we find to zeroth order

$$\left(\frac{\partial}{\partial t} - \frac{\partial \bar{p}}{\partial y}\frac{\partial}{\partial x}\right)\left[\psi_0 \frac{d^2\chi}{dx^2} + \chi\left(\frac{\partial^2 \psi_0}{\partial y^2} + \frac{1}{B}\frac{\partial^2 \psi_0}{\partial z^2}\right)\right] = 0. \tag{20}$$

The boundary conditions (14) and (15) give, to zeroth order,

$$\psi_0 = 0 \quad \text{on} \quad y = 0, q \tag{21}$$

because $\sin\phi = O(\epsilon) \times \sin\theta$, so that $|\cos\phi| = 1 - O(\epsilon^2)$. Separation of variables in (20) and use of the boundary conditions (21) give

$$\partial^2 \psi_0/\partial z^2 = h^2(\theta)\psi_0 \tag{22}$$

and

$$\frac{\partial^2 \psi_0}{\partial y^2} + \frac{n^2\pi^2}{q^2(\theta)}\psi_0 = 0, \tag{23}$$

so that

$$\psi_0 = [A_1 \cosh hz + A_2 \sinh hz]\sin(n\pi y/q), \tag{24}$$

where A_1, A_2, h and q are functions of θ. Equation (20) now reduces to

$$d^2\chi/d\theta^2 + \lambda^2(\theta)\,\epsilon^{-2}\chi = 0, \tag{25}$$

where

$$\lambda^2 = h^2/B - n^2\pi^2/q^2. \tag{26}$$

Since ϵ is small, (25) is of the standard form for a JWKB expansion with solution

$$\chi = \exp\left[\frac{i}{\epsilon}\int^{\theta} \Gamma(\theta)\, d\theta\right], \tag{27}$$

where

$$\Gamma = \pm\lambda + \frac{i\epsilon}{2\lambda}\frac{d\lambda}{d\theta} + O(\epsilon^2).$$

Boundary condition (16), to zeroth order, reduces to

$$\left(\frac{\Gamma z}{q}-\omega_0\right)\frac{\partial \psi_0}{\partial z}-\frac{\Gamma}{q}\psi_0=0 \quad \text{on} \quad z=\pm\tfrac{1}{2}. \tag{28}$$

Using the condition on $z=-\frac{1}{2}$ gives the ratio A_1/A_2 and we can put

$$A_1(\theta)=\frac{\Gamma}{q}\sinh\frac{h}{2}-h\left(\frac{\Gamma}{2q}+\omega_0\right)\cosh\frac{h}{2}, \tag{29}$$

$$A_2(\theta)=\frac{\Gamma}{q}\cosh\frac{h}{2}-h\left(\frac{\Gamma}{2q}+\omega_0\right)\sinh\frac{h}{2}. \tag{30}$$

The condition on $z=\frac{1}{2}$ gives another value for the ratio A_1/A_2 and elimination yields

$$\frac{q^2\omega_0^2}{\Gamma^2}=\frac{1}{h^2}-\frac{\coth h}{h}+\frac{1}{4}\equiv L(h^2). \tag{31}$$

The equation and boundary conditions for the first-order solution ψ_1 can be found from (7) and (14)–(17). Multiplication of this equation by ψ_0, integration with respect to y, z and θ and use of the boundary conditions yields a solubility condition which defines ω_1. The equation for ψ_1 can then be solved and thus further terms of the perturbation expansion can be obtained. Full details can be found in Gent (1974).

The radial velocity perturbation $v\equiv\partial p/\partial x$, so that the zeroth-order solution for v is

$$v=i\lambda^{\frac{1}{2}}[A_1\cosh hz+A_2\sinh hz]\sin\frac{n\pi y}{q}\exp\left[\pm\frac{i}{\epsilon}\int^{\theta}\lambda(\theta)\,d\theta-i\omega_0 t\right], \tag{32}$$

with

$$\omega_0^2=\left(\frac{1}{h^2}-\frac{\coth h}{h}+\frac{1}{4}\right)\left(\frac{h^2}{B}-\frac{n^2\pi^2}{q^2}\right)\frac{1}{q^2}\equiv\frac{L(h^2)\,\lambda^2}{q^2}. \tag{33}$$

It can be seen from the equation of motion and boundary conditions that, if $v(x, y, z)$ is an eigensolution with eigenvalue $\omega_0\equiv\omega_{0r}+i\omega_{0i}$, then so are

(*a*) $v(-x, y, z)$, with eigenvalue $-\omega_0$,

(*b*) $v(x, q-y, z)$, with eigenvalue ω_0,

(*c*) $v(x, y, -z)$, with eigenvalue $-\omega_0$,

(*d*) $v^*(x, y, z)$, with eigenvalue ω_0^*,

where an asterisk denotes a complex conjugate. If $q(\theta)$ were constant, the problem would reduce to Eady's and in that case there would be either one stable and one unstable mode or two neutral modes. If this is still true when q is a slowly varying function of x, then for $\omega_{0i}<0$ symmetries (*a*), (*c*) and (*d*) must give the same unstable mode. Thus if $\omega_{0i}\neq 0$, $-\omega_0=\omega_0^*$ and so $\omega_{0r}=0$. Thus ω_0^2 is always real and the principle of exchange of stabilities is valid. When q is not constant, however, the unstable mode could bifurcate into two unstable modes with distinct eigenvalues ω_0 and $-\omega_0^*$ (Drazin 1971), but in the following calculations only real values of ω_0^2 were used and the latter possibility ignored.

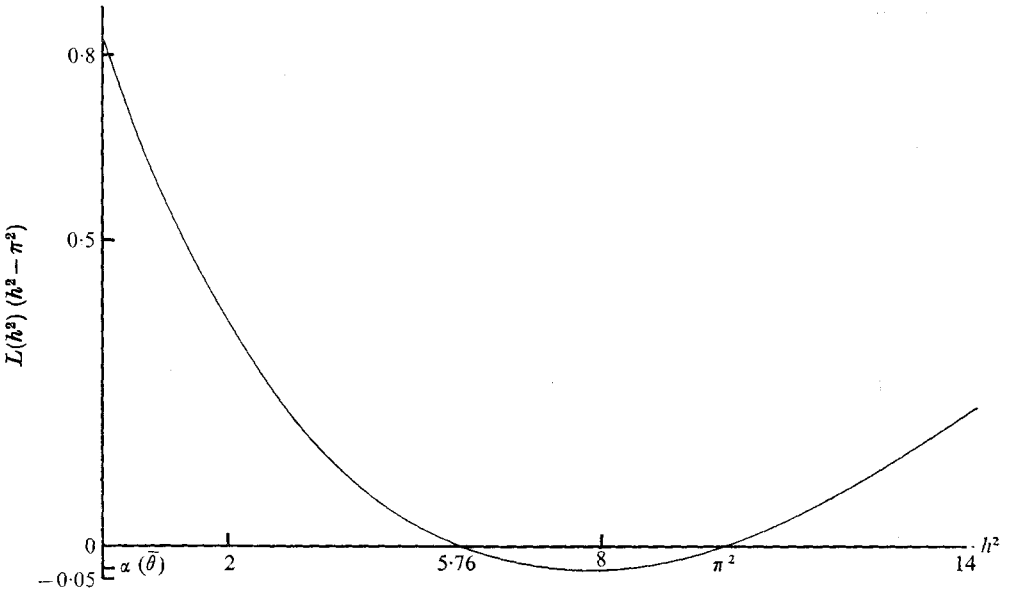

FIGURE 5. Graph of $L(h^2)\left(\frac{h^2}{B}-\frac{n^2\pi^2}{q^2}\right)\frac{1}{q^2}$ *vs.* h^2 for h^2 real with $B = n = q = 1$.

Global instability, $\omega_0^2 < 0$

In this section, the local stability characteristics are found when there is global instability. First assume a purely imaginary positive value for ω_0. (The reason for adopting this procedure is explained in § 5.) Then for given B and n, $h^2(\bar{\theta})$ can be found implicitly from (33) at any fixed value $\bar{\theta}$ of θ, and hence $\lambda^2(\bar{\theta})$ found from (26). The local stability characteristics at $\theta = \bar{\theta}$ depend on the nature of $\lambda^2(\bar{\theta})$. When $\omega_0^2 < 0$ there are three possible local stability regions and they can be seen by looking at the graph of ω_0^2 against h^2 for $\theta = \bar{\theta}$ and h^2 real. Figure 5 shows an example when $q(\bar{\theta}) = B = n = 1$. ω_0^2 has two zeros: when $L(h^2) = 0$, at $h^2 \simeq 5{\cdot}76$, and when $\lambda^2 = 0$, at $h^2 = Bn^2\pi^2q^{-2}$. The latter zero occurs at different values of h^2 depending on the value of $\bar{\theta}$. Define

$$\alpha(\bar{\theta}) = \min_{\substack{h^2 \text{ real} \\ -\pi^2 < h^2 < \infty}} \left[L(h^2)\left(\frac{h^2}{B}-\frac{n^2\pi^2}{q^2}\right)\frac{1}{q^2}\right]. \tag{34}$$

The minimum is taken between these limits on h^2 because the function tends to $+\infty$ as $h^2 \to +\infty$ and $-\pi^2$. The precise form of the graph of ω_0^2 against h^2, for h^2 real, depends upon $\bar{\theta}$ since q is a function of θ. When $Bn^2\pi^2q^{-2}(\bar{\theta}) < 5{\cdot}76$, $\alpha(\bar{\theta})$ is negative; it increases to zero as $Bn^2\pi^2q^{-2}(\bar{\theta}) \to 5{\cdot}76$, then decreases again and is negative when $Bn^2\pi^2q^{-2}(\bar{\theta}) > 5{\cdot}76$. If $Bn^2\pi^2q^{-2}(\bar{\theta}) < 5{\cdot}76$ and $\alpha(\bar{\theta}) < \omega_0^2$ then there are two possible real roots for h^2 and both give $\lambda^2(\bar{\theta})$ real and positive. The local solution for χ, therefore, is pure oscillatory and the flow is termed locally unstable. If $\alpha(\bar{\theta}) > \omega_0^2$ however, then the roots for h^2 and $\lambda^2(\bar{\theta})$ must be complex, the two roots being complex conjugates. The local solution for χ will now have both oscillatory and exponential terms, and is called damped oscillatory. Finally, if

$\alpha(\bar{\theta}) < \omega_0^2$ and $Bn^2\pi^2q^{-2}(\bar{\theta}) > 5{\cdot}76$, as in figure 5, then the two roots for h^2 are again real but both give $\lambda^2(\bar{\theta})$ real and negative. The local solution for χ, therefore, is exponentially decreasing and of the form

$$\chi \propto \exp\left[-(-\lambda^2(\bar{\theta}))^{\frac{1}{2}}\theta/\epsilon\right]. \tag{35}$$

The exponentially growing solutions have been neglected as they are physically inadmissible. Because ϵ is small, the spatial exponential decay of this final local solution means that it will be a small fraction of the order-one pure oscillatory spatial solution in the locally unstable region. This fraction is independent of the value of t and thus the flow is termed locally stable despite the exponential time growth of the linear solution. Drazin (1970) has studied the nonlinear Eady problem and showed that the separable, time-dependent part of the solution should not be exponentially growing, but is bounded above as $t \to \infty$. Thus the locally stable region, where the perturbation amplitude will always be small compared with that in the locally unstable region, corresponds to the symmetric flow in the experiments while the locally unstable region corresponds to the wave regime.

Let the boundaries between the locally unstable and damped oscillatory regions be at $\theta = \pm M$, and those between the damped oscillatory and locally stable regions at $\theta = \pm N$. Thus

$$\frac{Bn^2\pi^2}{q^2(\pm M)} < 5{\cdot}76 < \frac{Bn^2\pi^2}{q^2(\pm N)}, \quad \alpha(\pm M) = \alpha(\pm N) = \omega_0^2. \tag{36}$$

It can also be proved that there must be a region of local instability for the eigenfunction to be non-zero; if not, boundary condition (17) makes the eigenfunction identically zero.

If both M and N occur in the range $0 < \theta < \pi$ then the solution for v is

$$v \propto \begin{cases} i\lambda^{\frac{1}{2}} \exp\left[-\frac{1}{\epsilon}\int_{\theta}^{-M} \mathrm{Im}\,(\lambda)\,d\theta\right], & -\pi \leqslant \theta \leqslant -N, \\ i\lambda^{\frac{1}{2}} \exp\left[\frac{i}{\epsilon}\int_{-N}^{\theta} \mathrm{Re}\,(\lambda)\,d\theta\right] \exp\left[-\frac{1}{\epsilon}\int_{\theta}^{-M} \mathrm{Im}\,(\lambda)\,d\theta\right], & -N \leqslant \theta \leqslant -M, \\ i\lambda^{\frac{1}{2}} \exp\left[\frac{i}{\epsilon}\int_{-N}^{\theta} \mathrm{Re}\,(\lambda)\,d\theta\right], & -M \leqslant \theta \leqslant M, \\ i\lambda^{\frac{1}{2}} \exp\left[\frac{i}{\epsilon}\int_{-N}^{\theta} \mathrm{Re}\,(\lambda)\,d\theta\right] \exp\left[-\frac{1}{\epsilon}\int_{M}^{\theta} \mathrm{Im}\,(\lambda)\,d\theta\right], & M \leqslant \theta \leqslant N, \\ i\lambda^{\frac{1}{2}} \exp\left[\frac{i}{\epsilon}\int_{-N}^{N} \mathrm{Re}\,(\lambda)\,d\theta\right] \exp\left[-\frac{1}{\epsilon}\int_{M}^{\theta} \mathrm{Im}\,(\lambda)\,d\theta\right], & N \leqslant \theta \leqslant \pi. \end{cases} \tag{37}$$

Since λ^2 is an even function of θ and is real and negative when $N \leqslant \theta \leqslant \pi$, the boundary conditon $v(-\pi) = v(\pi)$ gives the eigenvalue relation

$$I \equiv \int_{-\pi}^{\pi} \mathrm{Re}\,(\lambda)\,d\theta = 2m\pi\epsilon, \tag{38}$$

for $m = 1, 2, 3, \ldots$, and the corresponding eigenfunction has $2m+1$ antinodes. This is the eigenvalue relation that determines whether the assumed value of ω_0 satisfies (38), and is indeed an eigenvalue.

If only the locally unstable and damped oscillatory regions occur, the solution for v is

$$v \propto \begin{cases} i\lambda^{\frac{1}{2}} \exp\left[\frac{i}{\epsilon}\int_{-\pi}^{\theta} \mathrm{Re}\,(\lambda)\,d\theta\right] \exp\left[-\frac{1}{\epsilon}\int_{\theta}^{-M} \mathrm{Im}\,(\lambda)\,d\theta\right], & -\pi \leqslant \theta \leqslant -M, \\ i\lambda^{\frac{1}{2}} \exp\left[\frac{i}{\epsilon}\int_{-\pi}^{\theta} \mathrm{Re}\,(\lambda)\,d\theta\right], & -M \leqslant \theta \leqslant M, \\ i\lambda^{\frac{1}{2}} \exp\left[\frac{i}{\epsilon}\int_{-\pi}^{\theta} \mathrm{Re}\,(\lambda)\,d\theta\right] \exp\left[-\frac{1}{\epsilon}\int_{M}^{\theta} \mathrm{Im}\,(\lambda)\,d\theta\right], & M \leqslant \theta \leqslant \pi. \end{cases} \tag{39}$$

The eigenvalue relation is again given by (38). If the solution for v is locally unstable everywhere, (38) is still the eigenvalue relation but the eigenfunction is

$$v \propto i\lambda^{\frac{1}{2}} \exp\left[\frac{i}{\epsilon}\int_{-\pi}^{\theta} \lambda\,d\theta\right], \quad -\pi \leqslant \theta \leqslant \pi, \tag{40}$$

which has $2m$ antinodes.

Global stability, $\omega_0^2 > 0$

When ω_0^2 is positive, (33) always gives two real roots for $h^2(\bar{\theta})$; see figure 5. For one of these roots $\lambda^2(\bar{\theta})$ is always negative and thus v is identically zero, but for the other root $\lambda^2(\bar{\theta})$ is always positive. The solution for v and the eigenvalue relation are given by (40) and (38) respectively. No profiles were calculated for the globally stable case.

5. Theoretical results

In order to find an eigenvalue, the values of B, m, n and ϵ must be known. The values from the experimental apparatus of $a = 51{\cdot}3$ mm, $b = 84{\cdot}3$ mm and $c = 9{\cdot}0$ mm were used, so that $\epsilon = 0{\cdot}3915$, which is rather large for use of the JWKB technique. The first mode, $n = 1$, is the most unstable. Then, for fixed values of B and m, a value was guessed for ω_0, the transition points at $\theta = \pm N$ found and the eigenvalue integral I evaluated using Gaussian integration. Linear interpolation on a few guesses quickly gave the value of ω_0 necessary to make $I = 2\pi m\epsilon$, and in this way the eigenvalue ω_0 was found as a function of the other parameters of the problem. When solving for λ^2 as a function of θ, there are always two roots. In the damped oscillatory region, choosing either of the complex-conjugate solutions does not alter the contribution to the eigenvalue integral I, but elsewhere one has to choose between the solutions. To ensure that $I \to 0$ as $\omega_0 \to 0$, one must choose the smaller root for λ^2 in the locally unstable region and the larger root in the locally stable region. Then $\lambda^2 \to 0$ as $\omega_0 \to 0$ for all θ and $\lambda^2 = 0$ on the neutral curve $\omega_0 = 0$.

To find the transition from an identically zero solution everywhere to a flow locally unstable only in the wide part of the channel, one has to find the value of B such that $I = 2\pi\epsilon$ when the point M occurs at $\theta = 0$. Then for B greater than

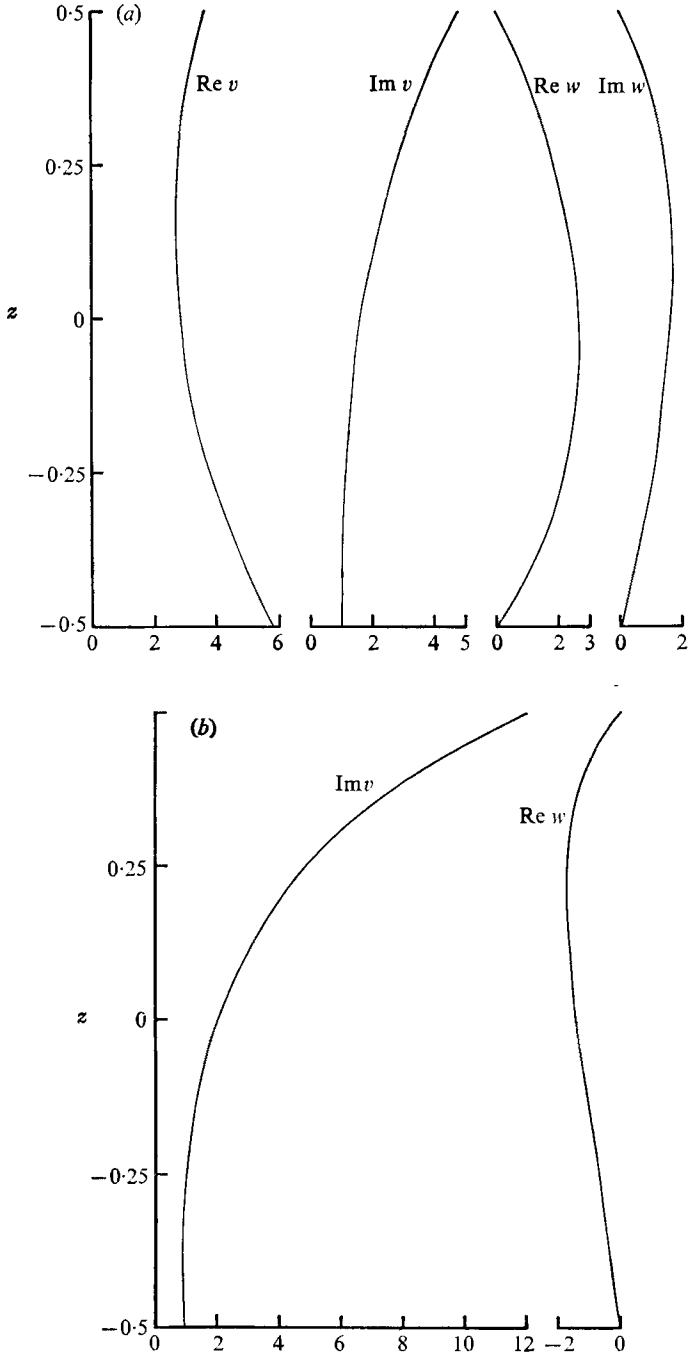

FIGURE 6. Vertical dependence of v and w at (*a*) the widest point and (*b*) the narrowest point; $B = 0{\cdot}722$, $\omega_0 = 0{\cdot}063i$, $m = 1$.

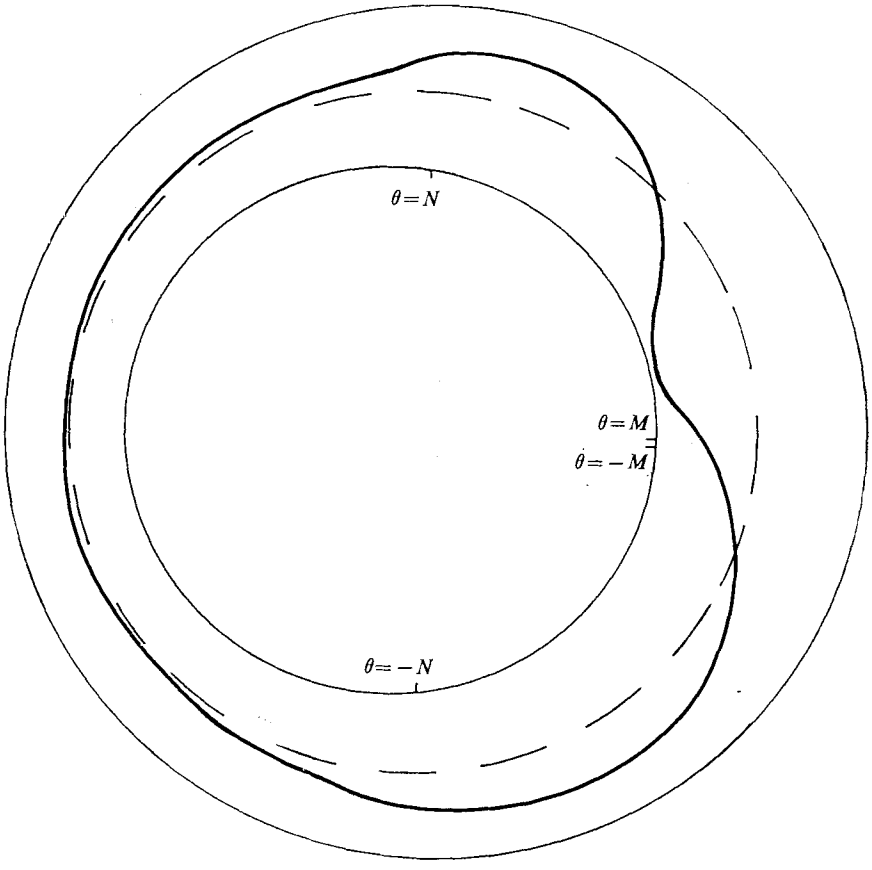

FIGURE 7. Azimuthal variation of v at mid-level; same case as figure 6.

this critical value, the flow is identically zero since there is no region of local instability, but for B less than this critical value, a flow can occur which is locally stable in the narrow region and locally unstable in the wide region. The theoretical value of B turns out to be 0·722, so that the critical local value at the widest point of the channel used in the experiments is $B_L(\epsilon, c) = 0{\cdot}446$ at this transition. This is somewhat lower than the inviscid Eady value of 0·583, to which it asymptotes as ϵ and $c \to 0$. Both values are shown on figure 2.

The vertically dependent part of the solution ψ_0 at this critical transition value of $B = 0{\cdot}722$ is illustrated in figure 6(*a*), which shows the real and imaginary parts of the eigenfunctions of the radial velocity v and the vertical velocity w at the widest point of the channel. From this the phase difference of v between the bottom and top of the model was found to be 0·75 rad. Figure 6(*b*) shows Im v and Re w at the narrowest point of the channel at the same critical value of B. At $\theta = \pi, \lambda^2$ is negative, so that Re v = Im $w \equiv 0$ and the phase difference of v between the bottom and top is zero. Both figures have been scaled such that Im $v = 1$ at the bottom of the annulus. Figure 7 shows the azimuthal variation of v at the mid-level of the fluid, $z = 0$, for the same critical value of B and $m = 1$.

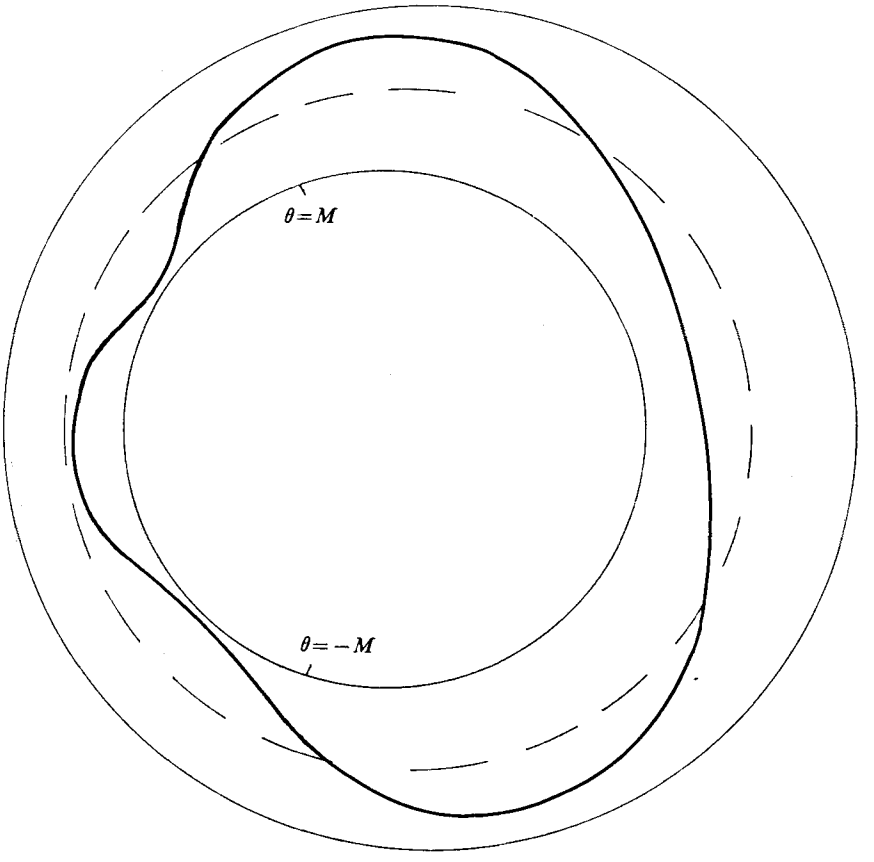

FIGURE 8. Azimuthal variation of v at mid-level; $B = 0{\cdot}36$, $\omega_0 = 0{\cdot}119i$, $m = 2$.

The inner and outer circles are drawn to scale with the experimental apparatus and the middle circle is the zero line for the radial velocity. v has been set positive at $\theta = 0$ and the amplitude scale varies linearly with the gap width q round the annulus. This solution for v is given by (37), and contains all three types of local behaviour, but the locally unstable region is very small since $M \simeq 1{\cdot}8°$. Figure 8 shows the eigenfunction for v at the mid-level with B_L at the widest point equal to 0·222 and $m = 2$. It is given by (39), and has only two types of local behaviour: locally unstable and damped oscillatory regions. The vertical phase difference is 1·61 rad at $\theta = 0$ and 0·17 rad at $\theta = \pi$. Figure 9 shows v at the mid-level of the fluid with B_L at the widest point equal to 0·123 and $m = 4$. This eigenfunction is given by (30), and is locally unstable at all azimuths. The vertical phase difference is 1·75 rad at $\theta = 0$ and 1·05 rad at $\theta = \pi$. The values of m used in calculating these eigenfunctions were chosen from the appropriate value for water–glycerol solution from table 1 for a given value of B_L. The vertical phase differences determined here are similar to those for the Eady model, which are shown in figure 2 of Douglas *et al.* (1972). They increase quickly at first as B_L decreases below the critical transition value but then increase very slowly as B_L decreases further.

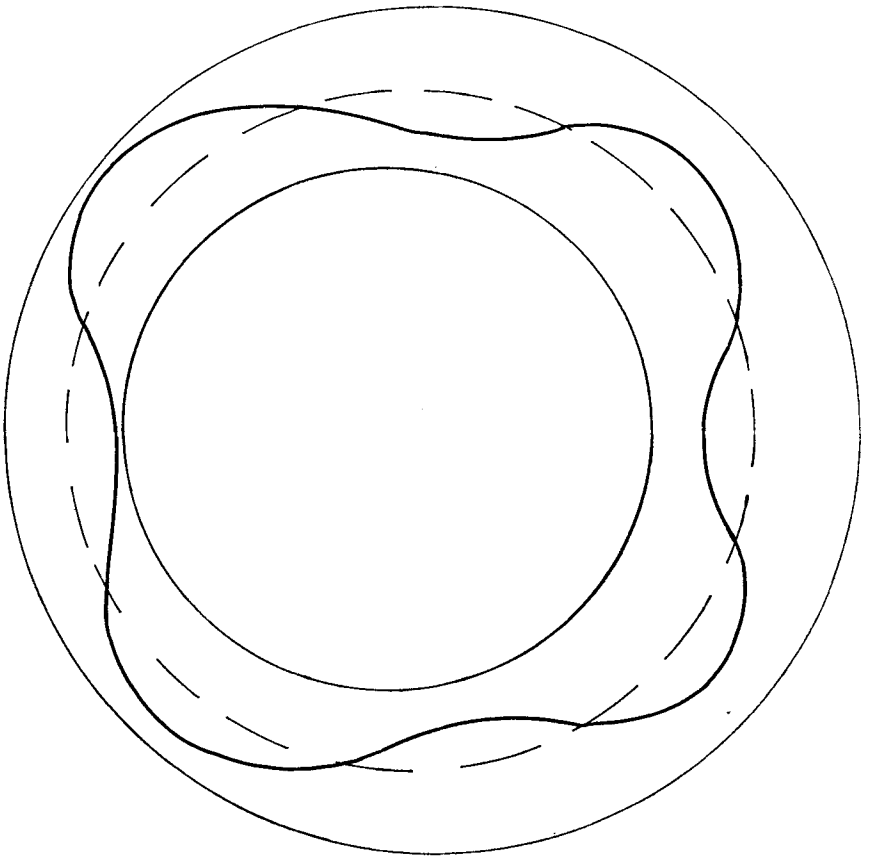

FIGURE 9. Azimuthal variation of v at mid-level; $B = 0{\cdot}2$, $\omega_0 = 0{\cdot}292i$, $m = 4$.

6. Conclusion

The laboratory experiments described above show that in an annulus whose channel width varies it is possible for baroclinic waves to occur locally depending predominantly upon the local value of the stability parameter B_L and the local Taylor number Ta_L. The flow can be symmetric everywhere or contain baroclinic waves everywhere, or else contain waves in the wide part of the annulus only with symmetric flow in the narrow part. The linear normal-mode analysis also predicts three different types of flow, and shows that the region of large meridional scale can be baroclinically unstable while the region of small scale is stable. To this extent there is qualitative agreement between the two investigations. The experiments show that, for the transition to waves in the wide part of the annulus, the critical value of B_L varies with viscosity, as in the concentric-annulus problem, whereas the inviscid theory predicts a single critical value of B_L, which lies within the range found experimentally for finite viscosity, again like the concentric case. Further quantitative comparison is inappropriate because of the inapplicability of the relatively simple theory to the more complicated, viscous, experimental situation.

We should like to acknowledge the guidance and encouragement given by Dr J. Brindley, Dr P. G. Drazin and Dr R. Hide and the assistance of various members of the Geophysical Fluid Dynamics Laboratory and the Meteorological Research and Development Workshop. We are grateful to Dr M. E. McIntyre for his help with the final preparation of this paper. We should also like to thank the Natural Environment Research Council for financial support.

REFERENCES

BARCILON, V. 1964 Role of Ekman layers in the stability of the symmetric regime obtained in a rotating annulus. *J. Atmos. Sci.* **21**, 291–299.

BRETHERTON, F. P. 1966 Critical layer instability in baroclinic flows. *Quart. J. Roy. Met. Soc.* **92**, 325–334.

BRINDLEY, J. 1960 Stability of flow in a rotating viscous incompressible fluid subjected to differential heating. *Phil. Trans.* A**253**, 1–25.

CHARNEY, J. G. 1947 The dynamics of longwaves in a baroclinic westerly current. *J. Met.* **4**, 135–163.

DAVIES, T. V. 1953 The forced flow of a rotating viscous liquid which is heated from below. *Phil. Trans.* A**246**, 81–112.

DAVIES, T. V. 1956 The forced flow due to heating of a rotating liquid. *Phil. Trans.* A**249**, 27–64.

DOUGLAS, H. A., HIDE, R. & MASON, P. J. 1972 An investigation of the structure of baroclinic waves using three-level streak photography. *Quart. J. Roy. Met. Soc.* **98**, 247–263.

DOUGLAS, H. A. & MASON, P. J. 1973 Thermal convection in a large rotating fluid annulus: some effects of varying the aspect ratio. *J. Atmos. Sci.* **30**, 1124–1134.

DRAZIN, P. G. 1970 Non-linear baroclinic instability of a continuous zonal flow. *Quart. J. Roy. Met. Soc.* **96**, 667–676.

DRAZIN, P. G. 1971 A note on a paper by Derome and Dolph. *Geophys. Fluid Dyn.* **2**, 185–187.

EADY, E. T. 1949 Longwaves and cyclone waves. *Tellus*, **1**, 33–52.

FOWLIS, W. W. & HIDE, R. 1965 Thermal convection in a rotating fluid annulus: effect of viscosity on the transition between axisymmetric and non-axisymmetric flow regimes. *J. Atmos. Sci.* **22**, 541–558.

FULTZ, D. 1949 A preliminary report on experiments with thermally produced lateral mixing in a rotating hemispherical shell of liquid. *J. Met.* **6**, 17–33.

FULTZ, D. 1951 Experimental analogues to atmospheric motions. *Compendium of Meteorology*, pp. 1235–1248. Boston: Am. Met. Soc.

FULTZ, D, LONG, R. L., OWENS, G. V., BOHAN, W., KAYLOR, R. & WEIL, J. 1959 Studies of thermal convection in a rotating cylinder with some implications for large-scale atmospheric motions. *Meteorol. Monographs*, vol. 4, no. 21. Boston: Am. Met. Soc.

GENT, P. R. 1974 Baroclinic instability of slowly varying flows. Ph.D. thesis, University of Bristol.

GREEN, J. S. A. 1960 A problem in baroclinic stability. *Quart. J. Roy. Met. Soc.* **86**, 237–251.

HIDE, R. 1953 Some experiments on thermal convection in a rotating liquid. *Quart. J. Roy. Met. Soc.* **79**, 161.

HIDE, R. 1958 An experimental study of thermal convection in a rotating liquid. *Phil. Trans.* A**250**, 442–478.

HIDE, R. 1969 Some laboratory experiments on free thermal convection in a rotating fluid subject to a horizontal temperature gradient and their relation to the theory of the global atmospheric circulation. In *The Global Circulation of the Atmosphere* (ed. G. A. Corby), pp. 196–221. London: Roy. Met. Soc.

HIDE, R. & MASON, P. J. 1970 Baroclinic waves in a rotating fluid subject to internal heating. *Phil. Trans.* A**268**, 201–232.

HIDE, R. & MASON, P. J. 1975 Sloping convection in a rotating fluid: a review. *Adv. in Phys.* **24**, 47–100.

KETCHUM, C. B. 1972 An experimental study of baroclinic annulus waves at large Taylor number. *J. Atmos. Sci.* **29**, 665–679.

LEACH, H. 1975 Thermal convection in a rotating fluid: effects due to non-axisymmetric boundaries. Ph.D. thesis, University of Leeds.

LORENZ, E. N. 1953 A proposed explanation for the existence of two regimes in a rotating symmetrically heated cylindrical vessel. In *Fluid Models in Geophysics* (ed. R. R. Long), pp. 73–80. U.S.A. Govt Printing Office.

MCINTYRE, M. E. 1970 On the non-separable baroclinic parallel flow instability problem. *J. Fluid Mech.* **40**, 273–306.

PEDLOSKY, J. 1964 The stability of currents in the atmosphere and the ocean. Part 1. *J. Atmos. Sci.* **21**, 201–219.

PEDLOSKY, J. 1970 Finite amplitude baroclinic waves. *J. Atmos. Sci.* **27**, 15–30.

PHILLIPS, N. A. 1963 Geostrophic motion. *Rev. Geophys.* **1**, 123–176.

WILLIAMS, G. P. 1971 Baroclinic annulus waves. *J. Fluid Mech.* **49**, 417–449.

WILLIAMS, G. P. 1974 Generalized Eady waves. *J. Fluid Mech.* **62**, 643–655.

WOOD, W. W. 1957 The asymptotic expansions at large Reynolds numbers for steady motions between non-coaxial rotating cylinders. *J. Fluid Mech.* **3**, 159–175.

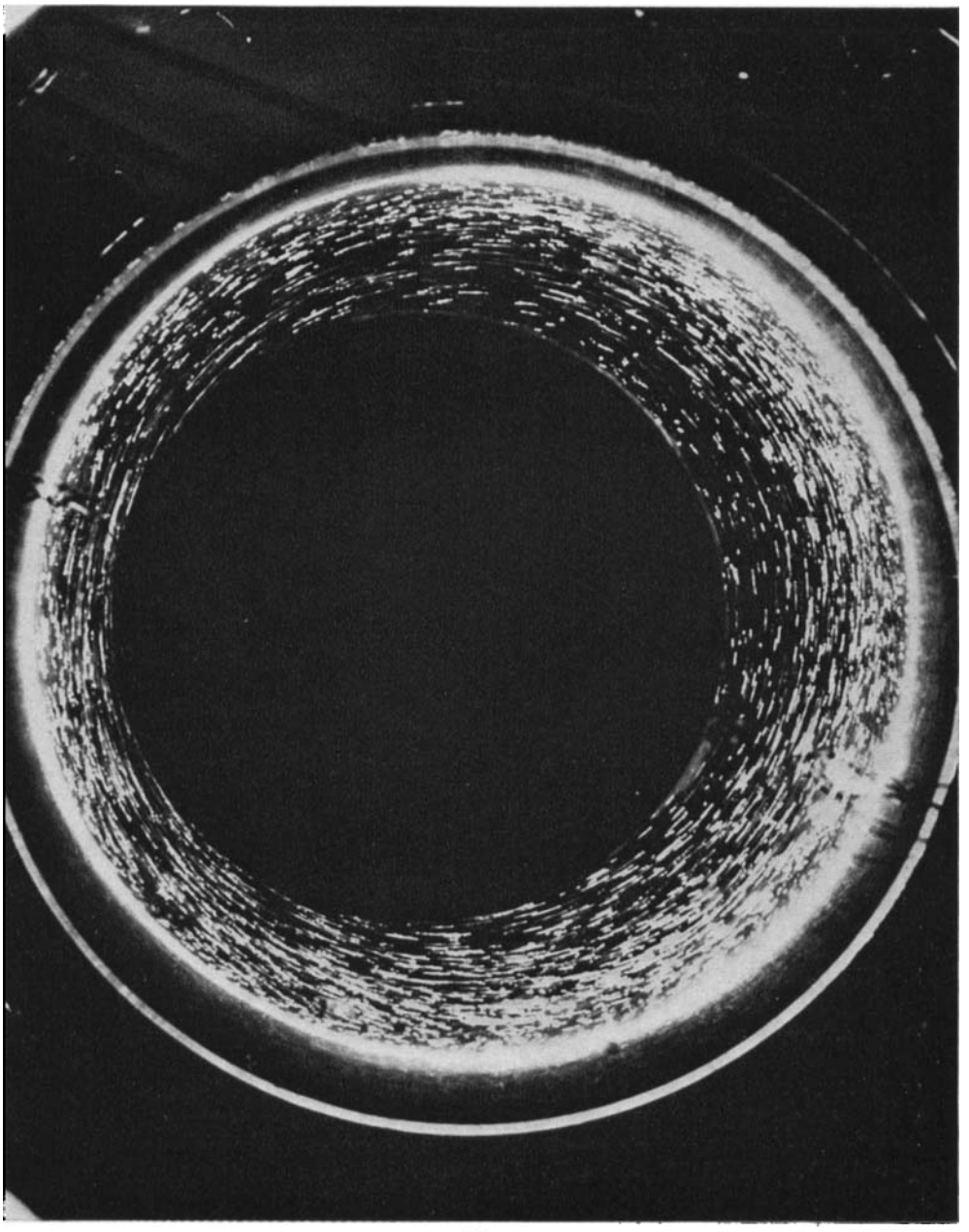

(*a*)

FIGURE 3. Streak photographs of flow patterns in water-glycerol solution near the mid-level of the fluid. 4 s exposure. (*a*) $\Omega = 0{\cdot}71$ rad s^{-1}, symmetric flow everywhere. (*b*) $\Omega = 1{\cdot}29$ rad s^{-1}, $m = 1$. (*c*) $\Omega = 1{\cdot}58$ rad s^{-1}, $m = 2$. (*d*) $\Omega = 1{\cdot}99$ rad s^{-1}, $m = 4$. (*e*) $\Omega = 2{\cdot}58$ rad s^{-1}, $m = 5$. (*b*) and (*c*) show waves only in the wide region while (*d*) and (*e*) show waves in the narrow region as well. Approximate values of B_L can be estimated from table 1.

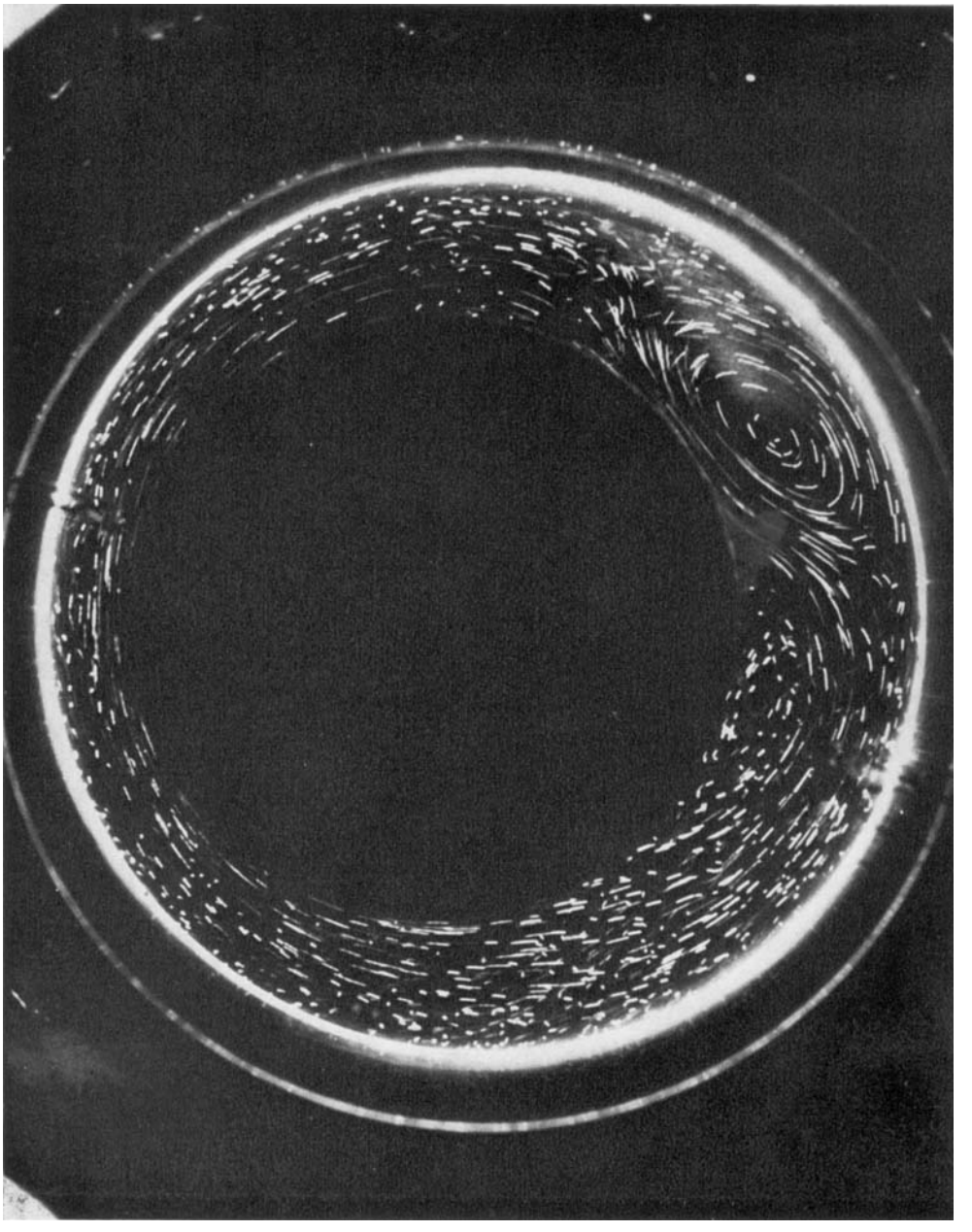

FIGURE 3(*b*). For legend see plate 1.

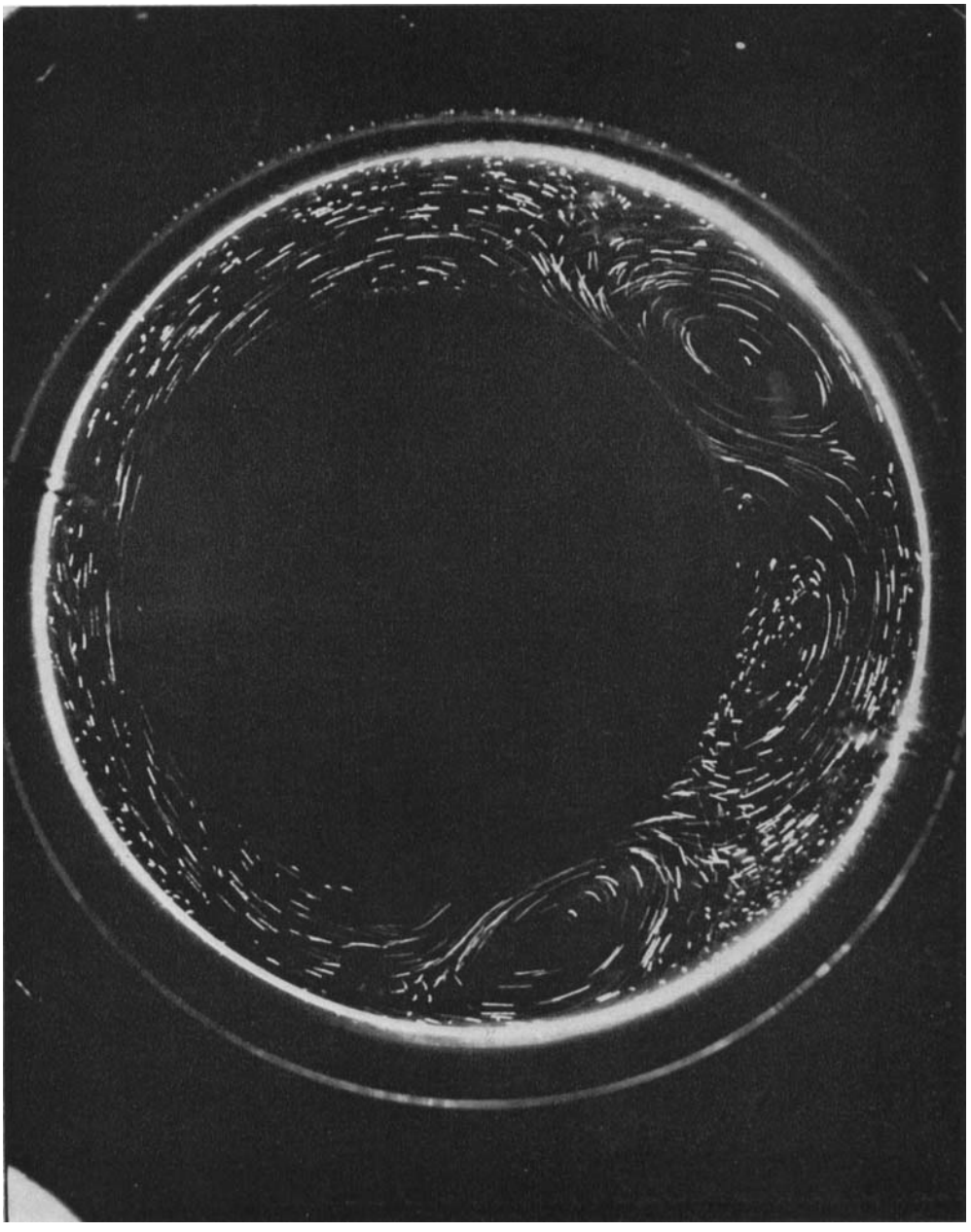

FIGURE 3(*c*). For legend see plate 1.

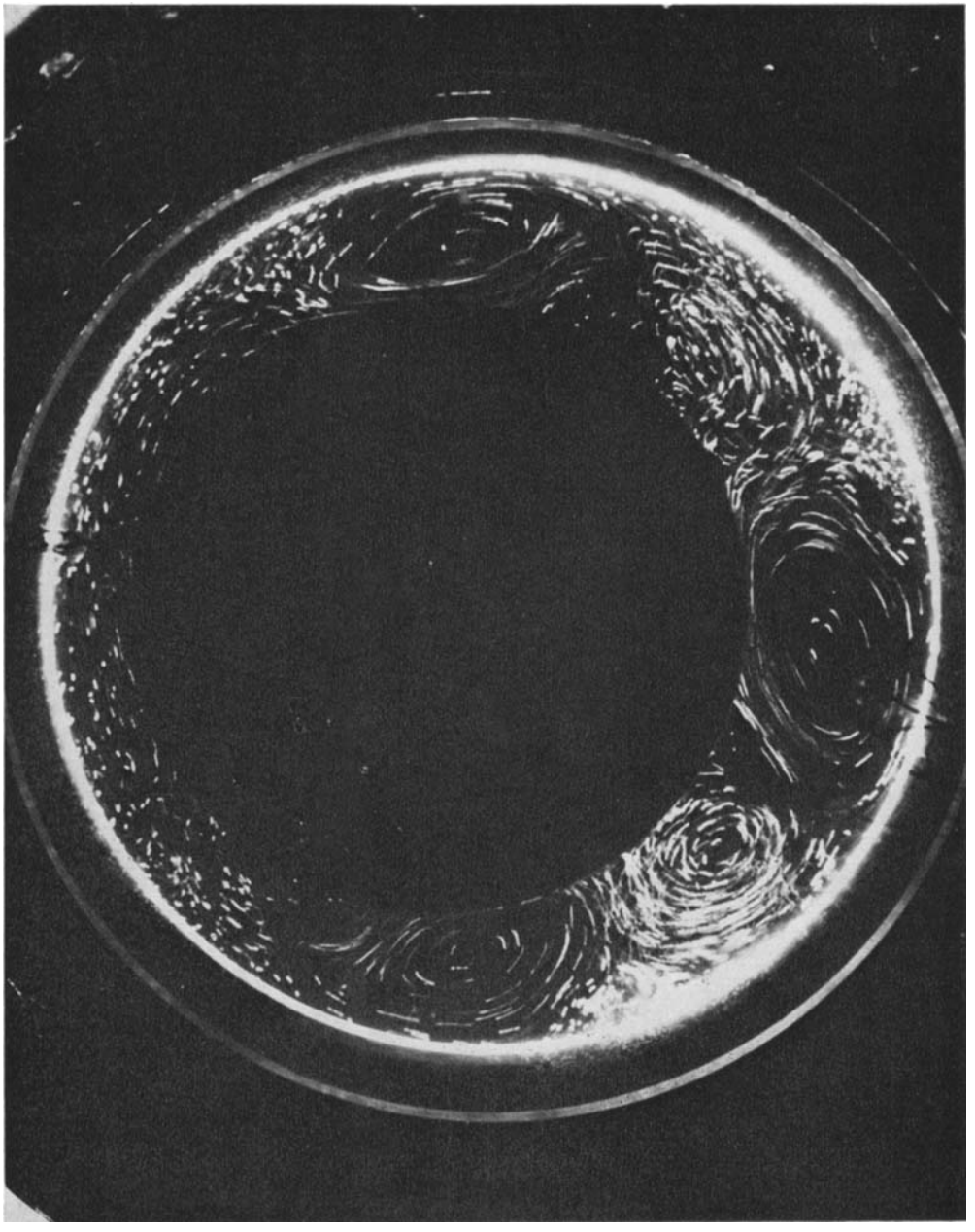

FIGURE 3(*d*). For legend see plate 1.

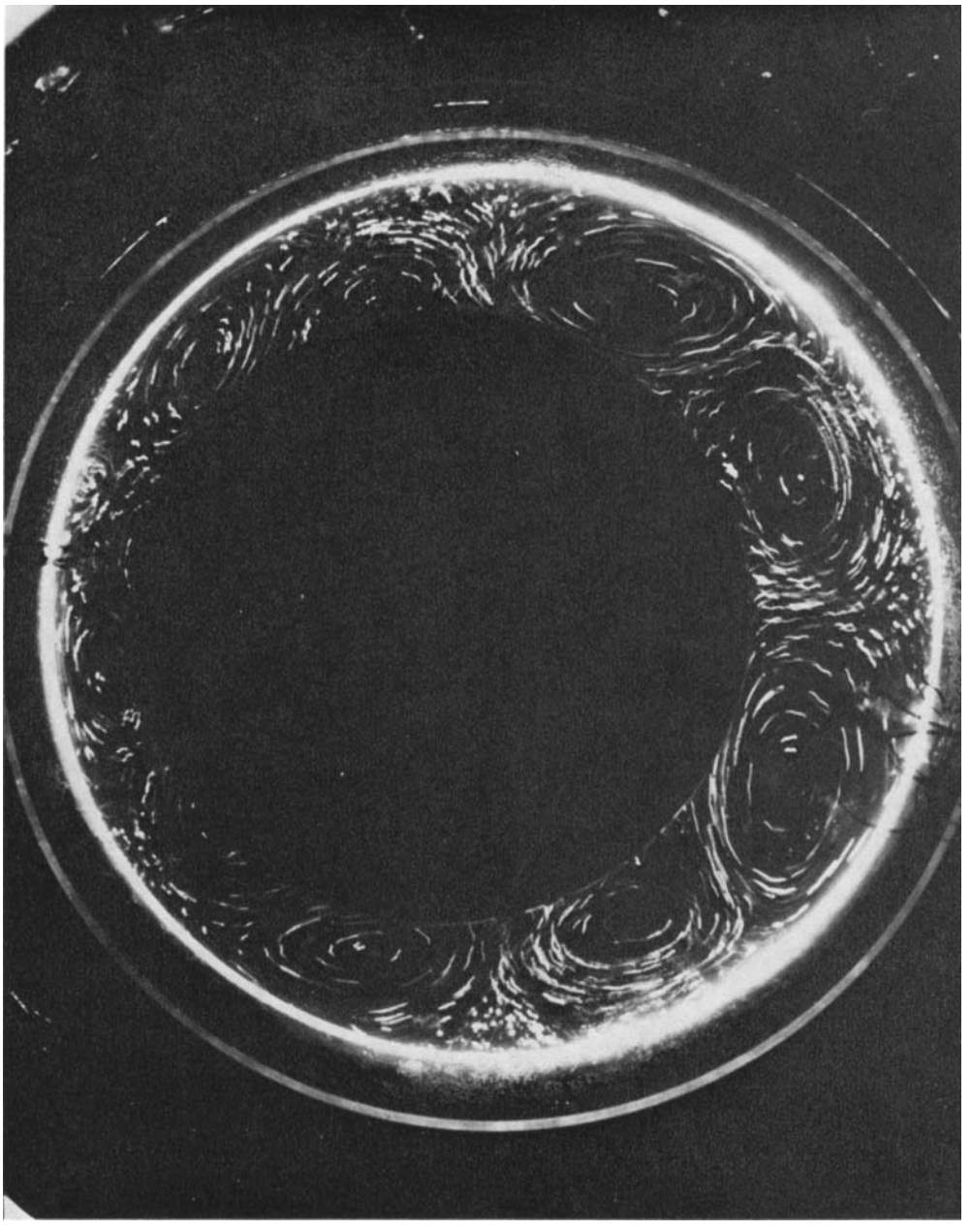

FIGURE 3(*e*). For legend see plate 1.